Optically Coherent Nitrogen-Vacancy Centers in Micrometer-Thin Etched Diamond Membranes

Ruf, Maximilian; Ijspeert, Mark; Van Dam, Suzanne; De Jong, Nick; Van Den Berg, Hans; Evers, Guus; Hanson, Ronald

DOI
10.1021/acs.nanolett.9b01316

Publication date
2019

Document Version
Final published version

Published in
Nano Letters

NANO LETTERS

Letter

Cite This: Nano Lett. 2019, 19, 3987−3992

pubs.acs.org/NanoLett

Optically Coherent Nitrogen-Vacancy Centers in Micrometer-Thin Etched Diamond Membranes

Maximilian Ruf,[†,‡,⊥] Mark IJspeert,[†,‡,∥,⊥] Suzanne van Dam,[†,‡] Nick de Jong,[†,§] Hans van den Berg,[†,§] Guus Evers,[†,‡] and Ronald Hanson*[,†,‡]

[†]QuTech and [‡]Kavli Institute of Nanoscience, Delft University of Technology, 2628 CJ Delft, The Netherlands

[§]Netherlands Organisation for Applied Scientific Research (TNO), 2628 CK Delft, The Netherlands

Supporting Information

ABSTRACT: Diamond membrane devices containing optically coherent nitrogen-vacancy (NV) centers are key to enable novel cryogenic experiments such as optical ground-state cooling of hybrid spin-mechanical systems and efficient entanglement distribution in quantum networks. Here, we report on the fabrication of a (3.4 ± 0.2) μm thin, smooth (surface roughness $r_q < 0.4$ nm over an area of 20 μm by 30 μm) diamond membrane containing individually resolvable, narrow linewidth (< 100 MHz) NV centers. We fabricate this sample via a combination of high-energy electron irradiation, high-temperature annealing, and an optimized etching sequence found via a systematic study of the diamond surface evolution on the microscopic level in different etch chemistries. Although our particular device dimensions are optimized for cavity-enhanced entanglement generation between distant NV centers in open, tunable microcavities, our results have implications for a broad range of quantum experiments that require the combination of narrow optical transitions and micrometer-scale device geometry.

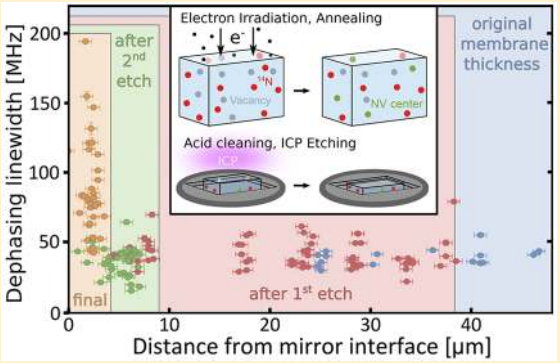

KEYWORDS: *Nitrogen-vacancy center, diamond nanofabrication, electron irradiation, optical coherence, quantum information science*

The negative nitrogen-vacancy (NV) center is a point defect center in diamond[1,2] that is used in a wide range of experiments, including quantum sensing,[3−7] quantum computation algorithms,[8,9] and quantum communication.[10−12] In addition to second-long spin coherence times[13] and spin-conserving optical transitions,[14] NV centers feature coupling to nearby nuclear spins that can act as memory quantum bits.[11,15,16] Many NV-based experiments require a combination of good optical and spin properties in nanofabricated structures; these experiments include Purcell enhancement of the optical zero-phonon line (ZPL) transitions in a diamond microcavity[17−30] for entanglement generation speed-up, optical ground-state cooling of a hybrid NV-cantilever spin-mechanical system,[31−36] and resonant optical readout of NV centers in sensing applications.[14] Although good spin coherence has been demonstrated for surface-proximal NVs (depth of ∼50 nm),[37−39] the incorporation of optically coherent NV centers in micrometer-scale devices remains an outstanding challenge.

The optically excited state of the NV center is sensitive to electric fields and crystal strain.[40] Therefore, high-frequency electric-field noise can lead to dephasing in the excited state, whereas on longer timescales the transitions can be effectively widened by slow spectral diffusion originating from a changing charge state distribution in the environment.[41,42] Although the latter effect can be mitigated by actively tracking the transition frequencies and adding feedback,[10] it comes at the cost of reduced experimental repetition rates. Dephasing poses a more fundamental challenge. In hybrid-mechanical systems, effective optical ground-state cooling requires operation in the sideband resolved regime.[31,34] Dephasing also determines the resolvable magnetic field changes in sensing experiments and limits the two-photon quantum interference contrast that translates into state fidelity for entanglement protocols.[43,44] For all discussed applications of NV centers in membranes, spectral diffusion widths <250 MHz and dephasing widths <100 MHz are in practice desired.[45] However, reported spectral diffusion widths in thin (∼1 μm) nanofabricated structures are ∼1 GHz[30] for NV centers formed via nitrogen implantation.[46] Improvements in fabrication and preparation methods are therefore necessary to produce devices with linewidths sufficiently narrow for the experiments discussed above.

For our desired application of embedding a diamond membrane in an open, tunable Fabry−Perot microcavity to increase entanglement generation rates between distant NV centers,[28−30,47,48] we target a final membrane thickness of ∼4 μm. This choice is a compromise between low cavity mode volume needed for high Purcell enhancement and sufficient

Received: March 30, 2019
Revised: May 15, 2019
Published: May 28, 2019

DOI: 10.1021/acs.nanolett.9b01316
Nano Lett. 2019, 19, 3987−3992

thickness to avoid frequent breaking of membranes during sample handling, while being able to embed NVs as deep in the diamond lattice as possible to avoid surface-induced noise. We furthermore require smooth samples (r_q < 0.3 nm over the ~4 μm^2 large area of the cavity beam waist) to limit losses due to scattering at the diamond−air interface (scaling with r_q squared).[47,49]

Here, we report on a full fabrication procedure that combines high-energy electron irradiation, high-temperature annealing, and an optimized etching sequence to yield a diamond device that meets all the above requirements. We verify the desired NV center optical properties using an extensive study on linewidths following different etching steps.

We start from an ultrapure, CVD-grown diamond that contains only a few NV centers[45] and thus requires their density to be increased. NV centers created from implanted nitrogen atoms were recently found to predominately feature broad optical lines, likely due to associated diamond lattice damage.[50] Instead, we use high-energy electron irradiation to create vacancies throughout the whole diamond that can form NV centers with native nitrogen (see Figure 1A).[51] After

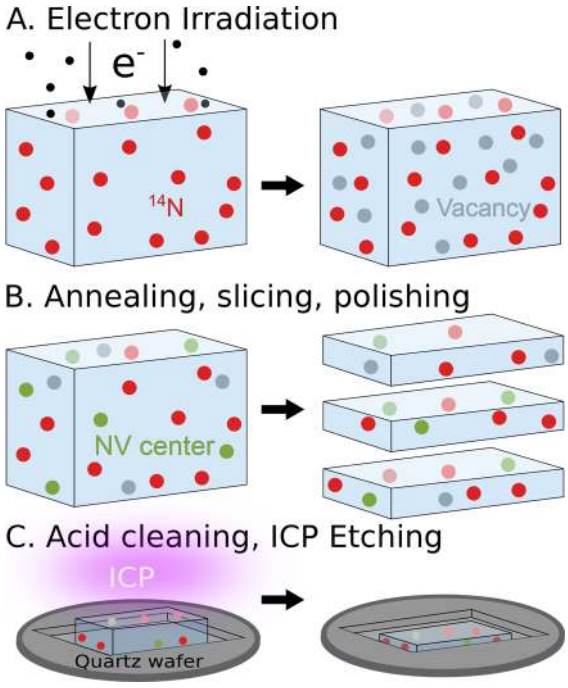

Figure 1. Schematic of the diamond fabrication process flow. (A) A CVD-grown diamond is irradiated with electrons to form vacancies in the diamond lattice.[45] (B) After a triacid clean, a high-temperature annealing process in high vacuum combines the holes with naturally occurring nitrogen in the sample to form NV centers.[45] The sample is then sliced into three 50 μm thick slabs that are each polished to a surface roughness of typically r_q < 1 nm. (C) After an acid clean to remove the remaining contamination that could lead to masking during etching, the sample is etched in an ICP-RIE.

triacid cleaning, a high-temperature and high-vacuum annealing sequence, consisting of three temperature steps, ensures the recombination of vacancies with naturally occurring nitrogen in the diamond to form NV centers and anneals out vacancy chains (see Figure 1B).[52,53] The resulting density of NV centers thus depends on the nitrogen distribution resulting from diamond growth and the number of vacancies created during electron irradiation.[45] The diamonds are subsequently sliced and polished into three membranes of ~50 μm thickness each. This value is a trade-off between ease of handling of the membranes in further processing steps, and the amount of material that needs to be removed in a subsequent reactive ion etching (RIE) step using inductively coupled plasma (ICP) (see Figure 1C).

To find an etch recipe that leads to smooth, thin diamonds, we investigate the effect of different etch chemistries on the diamond surface roughness on the microscopic level. It is advantageous to employ an oxygen-based ICP-RIE, due to reported high diamond etch rates (>200 nm/min),[54] and an oxygen-rich surface termination of the diamond, which is beneficial for the charge state stability of the NV^- center.[55] However, it has been speculated that particles, for example those introduced during diamond polishing, wet-processing, or sample handling,[45] can lead to hole formation during etching with O_2.[56,57]

By overlaying atomic force microscope (AFM) surface images of identical diamond areas before and after O_2 etching, we find that each of the observed circular pits originates from a particle that was initially present at that location. Figure 2

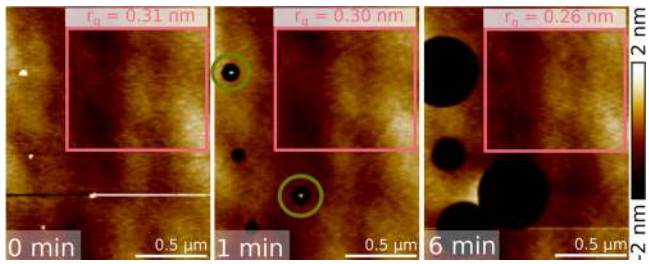

Figure 2. Evolution of a diamond surface during ICP-RIE with O_2 for different etching times (indicated in the bottom left corner of each AFM image for an identical area). The data demonstrates that debris on the diamond surface leads to micromasking during etching, resulting in the formation of nanopillars (visible in the green encircled parts after 1 min of etching). These pillars are subsequently removed via an isotropic etch component. Pink rectangles show a comparison of surface roughness r_q for a 1 μm by 1 μm wide area that excludes etch-induced holes (error 0.03 nm). Note that the black/white trace in the AFM image before etching is a data acquisition artifact.

shows the evolution of one such area before etching, and after 1 and 6 min of etching with O_2.[45] The data demonstrates that the underlying mechanism of hole formation is micromasking: the particle etch rate is lower than that of the bulk diamond surface. This leads to the formation of diamond nanopillars on the surface that deflect the impinging plasma, which enhances the etch rate locally and thus creates a hole around the pillar[54] (see the green encircled areas in Figure 2 after 1 min of etching). Because of an isotropic etch component, the pillars are eventually etched away, leaving behind a hole. These holes then remain and widen as the etching continues. Importantly, we also find that the membrane surface roughness can be maintained during O_2 etching if particle-induced holes are excluded (see the pink rectangles in Figure 2). Even after extended O_2 etches, one thus expects to maintain the intitial diamond surface roughness if particles can be effectively removed before this step.

To reduce the number of particles on the diamond surface to levels lower than after acid cleaning alone,[45] common strategies are to etch under Ar/Cl_2[58] or SF_6.[59] However, Ar/Cl_2 etching induces Cl contamination on the diamond

DOI: 10.1021/acs.nanolett.9b01316
Nano Lett. 2019, 19, 3987−3992

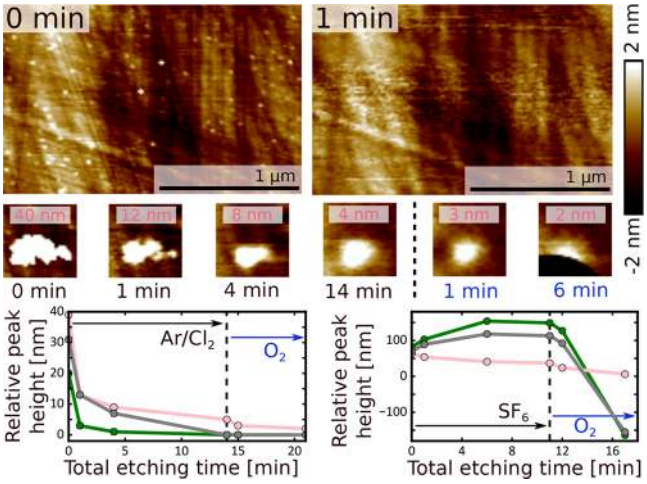

Figure 3. Evolution of particles and surface roughness during etching with Ar/Cl_2 of a diamond surface and relative particle height versus etching time for SF_6 and Ar/Cl_2 etching. Top row of AFM images demonstrates that 1 min of Ar/Cl_2 etching effectively removes small particles. Middle row of AFM images (1 μm by 1 μm) shows the evolution of the relative peak height of an initially large particle with respect to the mean surface height as a function of etching time during etching with Ar/Cl_2 (black time indication) and subsequent with O_2 (blue indication), respectively. Note that the big hole after 6 min of etching with O_2 results from etch-induced widening of an initially present hole on the diamond surface, caused by a low-quality diamond growth and polishing process.[45] Bottom graphs compare relative peak height (or hole depth) evolution under $ArCl_2$ (left graph) and SF_6 (right graph) pre-etching, followed by O_2 etching for different selected particles (see ref 45 for the full underlying data set).

surface,[60] which is suspected to have a detrimental influence on the optical and spin properties of NV centers. Therefore, Ar/Cl_2 is often combined with O_2 etching.[7,30,53,59,61,62] Figure 3 confirms that Ar/Cl_2 is indeed highly effective in removing particles, and that it can be followed by O_2 etching without forming holes on the surface. By comparing the evolution of the relative peak height of particles with respect to the mean of the surrounding diamond surface (see Figure 3, bottom graphs), we find that Ar/Cl_2 is more efficient in removing particles from the diamond surface than SF_6;[45] although Ar/Cl_2 removes small particles within the first minute of etching and continues to reduce the relative peak height of large debris for longer etching times, it takes longer for small particles to be removed in SF_6 and the relative peak height of some larger remaining structures increases during etching in this chemistry, leading to the formation of holes.

Using the above etch recipe, we fabricate a sample following the steps in Figure 1. For microwave delivery and repeated identification of the measurement area, the sample is bonded via van der Waals forces to a superpolished mirror patterned with golden striplines and unique position markers before etching.[63] We have observed that the exposure of mirror material to the plasma leads to severe micromasking on the diamond as etched mirror material is redeposited on the diamond surface. This results in the formation of holes on the diamond following the same mechanism as discussed above. To mitigate this effect, we use a fused quartz mask for partial exposure of the diamond[62] (see Figure 4 (top left)). We thin the sample in three etching steps, each consisting of an Ar/Cl_2 pre-etch, followed by a single O_2 step, for a total etch duration of 86 min of Ar/Cl_2 and 206 min of O_2 etching. Figure 4

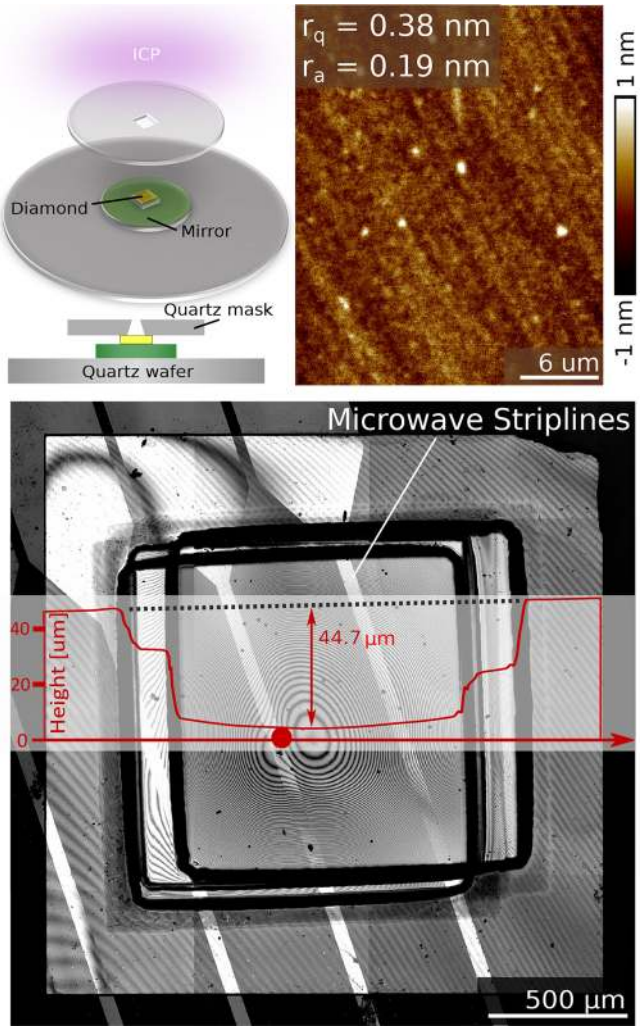

Figure 4. Schematic of the diamond etching setup and resulting membrane profile. (Top left) Setup used for bonded diamond etching. A diamond membrane is bonded to a mirror patterned with gold position markers and striplines, positioned on a fused quartz carrier wafer, and masked from the top with a fused quartz substrate that has a rectangular opening.[45,62] (Bottom) Confocal microscope image of an etched diamond membrane with three clearly visible offset recesses that result from repeated and shifted partial exposure. The red arrow indicates the profilometer path along which a height profile (red) was taken. It reveals a diamond wedge of 0.14° (angle of dotted line with respect to the horizontal axis) resulting from the diamond slicing and polishing process, and a maximum etch depth of (44.7 ± 0.2) μm in the middle region. The red circle corresponds to the region within which most of the data in this paper was taken with a final thickness of (3.8 ± 0.2) μm. The fringe spacing corresponds to a height change of 84 nm. (Top right) AFM image of the region indicated with a red circle in the middle image, showing a low surface roughness of r_q = 0.38 nm over an area of 20 μm by 30 μm.

(bottom) shows a confocal microscope image and stylus profilometer height trace of the bonded membrane after the full etching sequence. The geometry of the mask restricts the solid angle of incidence and leads to a position-dependent etch rate. Therefore, the sample height profile shows a curvature in the exposed region with a thinnest membrane thickness of (3.4 ± 0.2) μm. The red dot indicates the (3.8 ± 0.2) μm thick area within which the AFM image in Figure 4 (top right) was taken after the full etch. This image confirms a smooth diamond

DOI: 10.1021/acs.nanolett.9b01316
Nano Lett. 2019, 19, 3987−3992

surface (r_q = 0.38 nm over a 20 μm by 30 μm area) even after this prolonged etch sequence.

We characterize the optical properties of NV centers in between etch steps in a confocal microscopy setup <10 K by using a largely automatized measurement sequence to determine their linewidths via photoluminescence excitation (PLE) scans of the ZPL transitions.[45] After roughly localizing an NV transition in frequency space, we scan a tunable laser around this frequency, while detecting photons emitted from the NV in the phonon sideband (PSB). We repeatedly apply a sequence of a short green laser pulse (to ensure spin and charge state initialization), followed by a red frequency sweep through the expected transition frequency (to map out the specific ZPL transition under dephasing). We do this while constantly applying microwaves to avoid pumping in an optically dark spin state. By performing many scans of this kind, we probe both the effects of spectral diffusion (via a fit to the averaged counts of all scans), as well as the average dephasing width (by fitting each scan individually and calculating the weighted mean for all fitted linewidths).

Figure 5 shows the results of spectral diffusion and dephasing widths as a function of distance from the mirror

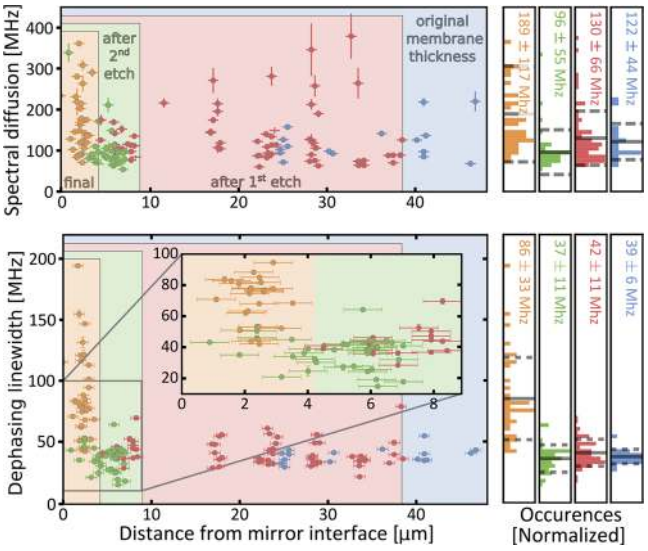

Figure 5. Overview of spectral diffusion (top left panel) and dephasing linewidth (bottom left panel) of NV centers at various distances from the mirror interface for different membrane thicknesses. Right hand side shows normalized histograms of the data on the left, with the black solid (dashed) lines visualizing the mean (standard deviation) of the data for a given membrane thickness, and the colored numbers indicating these values. (Blue) Data before any etching, membrane thickness in measurement region t_m = (47.8 ± 0.2) μm. (Red) Data after first etching of 26 min Ar/Cl_2, followed by 45 min of O_2, t_m = (37.7 ± 0.2) μm. (Green) Data after an additional 30 min Ar/Cl_2 and 138 min O_2 etching, t_m = (10.1 ± 0.2) μm. (Yellow) Data after an additional 30 min Ar/Cl_2 and 23 min O_2 etching, t_m = (3.8 ± 0.2) μm. The horizontal clustering of points is a data acquisition artifact.

interface for a total of 155 NV center transitions, stemming from 110 distinguishable NV centers. This data has been acquired at four different steps during membrane thinning and thus membrane thicknesses t_m in the measurement region. Although we are not able to track identical NV centers throughout the different etch steps, we make sure to look at the same 20 μm by 20 μm area of diamond for all measurements, apart from the data for the thinnest membrane, for which we additionally included a second region ~200 μm from the main measurement area for increased statistics. Confocal scans performed after each etching step show no evidence of strong variations in NV center density.

The data shows the potential of electron irradiation as a reliable way of introducing coherent NV centers throughout the membrane. For the unetched case, we find an average dephasing width of (39 ± 6) MHz, and an average spectral diffusion width of (122 ± 44) MHz. We suspect that laser-power-induced line width broadening prevents us from resolving lifetime limited values for the dephasing line widths.[45] Importantly, for membranes etched down to t_m = (37.7 ± 0.2) μm and to t_m = (10.1 ± 0.2) μm, we observe that all linewidth averages overlap within statistical uncertainties.

We find roughly two times broader linewidths when characterizing NVs at the final membrane thickness of t_m = (3.8 ± 0.2) μm in the measurement region; the spectral diffusion width averages to (189 ± 117) MHz, whereas the dephasing width averages to (86 ± 33) MHz. Yet, even for this thickness, we find that 22 out of 37 measured NV centers fulfill our preset criteria of dephasing linewidth <100 MHz and spectral diffusion line width <250 MHz. Possible mechanisms that could explain this line width broadening after the last etching step include additional dephasing due to Cl residue left behind on the diamond surface after the proportionally longer etching under Ar/Cl_2 for this final etch step, as well as lattice damage induced by reflection of ions from the diamond–mirror interface.

The NV ZPL transitions shift with crystal strain. Although axial strain results in an overall resonance frequency shift, transverse strain splits the E_x and E_y optical transitions.[1] To determine whether strain in the diamond influences the observed linewidth broadening, we extract the transverse and axial strain from a subset of NV centers via a reconstruction of the NV center Hamiltonian.[45] Although the average axial and transverse strain increase with decreasing NV distance from the mirror interface, the data does not show a dependency of the measured spectral diffusion and dephasing linewidths on strain,[45] suggesting that there is no direct causal relation between the two. Possible causes of increased strain found for NVs after the last etching step include a stressed layer that remains after the membrane polishing process,[64−66] effects due to bonding of the diamond to the mirror (including stress resulting from the difference in thermal expansion coefficients for the diamond and mirror), and lattice-damage induced by reflected ions as discussed above. Future systematic studies beyond the current work are required to pinpoint the origin unambiguously.

In conclusion, we have demonstrated the fabrication of a diamond sample with a high density of NV centers, introduced through electron irradiation and subsequent high-temperature annealing. The surface roughness (r_q < 0.4 nm for a 20 μm by 30 μm area), thickness (~4 m), and NV linewidths (<100 MHz) of this sample allow for enhanced entanglement generation rates via the Purcell effect in an open, tunable microcavity setup. Given these sample properties and vibration levels of 0.1 nm rms under pulse-tube operation,[48] we expect an emission of ZPL photons coupled into the fiber mode of 35%,[49] which translates into an entanglement rate enhancement of 2 orders of magnitude. This would allow one to form a quantum repeater beating direct transmission,[67−69] signaling

DOI: 10.1021/acs.nanolett.9b01316
Nano Lett. 2019, 19, 3987−3992

the surpassing of a fundamental milestone on the route to building a quantum network.

■ ASSOCIATED CONTENT

Supporting Information

The Supporting Information is available free of charge on the ACS Publications website at DOI: 10.1021/acs.nanolett.9b01316.

Details on sample preparation and etch recipe development. Fabrication of sample described in main text. NV line width characterization methods. Laser-power-induced line width broadening. NV depth conversion factor and error analysis. Correlations of NV center strain and line widths (PDF)

■ AUTHOR INFORMATION

Corresponding Author

*E-mail: r.hanson@tudelft.nl.

ORCID

Maximilian Ruf: 0000-0001-9116-6214

Suzanne van Dam: 0000-0001-9814-3162

Present Address

∥(M.I.) Clarendon Laboratory, Parks Road, Oxford OX1 3PU, United Kingdom.

Author Contributions

⊥M.R. and M.I. contributed equally to this work.

Notes

The authors declare no competing financial interest.

■ ACKNOWLEDGMENTS

The authors thank Marinus Hom, Wybe Roodhuyzen, and Ferdinand Grozema for electron irradiation of diamonds, Kevin Chang, Michael Burek, Daniel Riedel, and Erika Janitz for helpful nanofabrication discussions, Charles de Boer, Eugene Straver, Marc Zuiddam, and Jasper Flipse for fabrication assistance, Airat Galiullin for developing early versions of the measurement scripts, and Matthew Weaver and David Hunger for careful reading of our manuscript. This research was supported by the Early Research Programme of The Netherlands Organisation for Applied Scientific Research (TNO) and by the Top Sector High Tech Systems and Materials. We furthermore acknowledge financial support from The Netherlands Organisation for Scientific Research (NWO) through a VICI Grant and from the European Research Council through an ERC Consolidator Grant.

■ REFERENCES

(1) Doherty, M. W.; Manson, N. B.; Delaney, P.; Jelezko, F.; Wrachtrup, J.; Hollenberg, L. C. L. *Phys. Rep.* **2013**, *528*, 1−45.

(2) Atatüre, M.; Englund, D.; Vamivakas, N.; Lee, S. Y.; Wrachtrup, J. *Nature Reviews Materials* **2018**, *3*, 38−51.

(3) Degen, C. L. *Appl. Phys. Lett.* **2008**, *92*, 243111.

(4) Maze, J. R.; Stanwix, P. L.; Hodges, J. S.; Hong, S.; Taylor, J. M.; Cappellaro, P.; Jiang, L.; Dutt, M. V.; Togan, E.; Zibrov, A. S.; Yacoby, A.; Walsworth, R. L.; Lukin, M. D. *Nature* **2008**, *455*, 644−647.

(5) Balasubramanian, G.; Chan, I. Y.; Kolesov, R.; AlHmoud, M.; Tisler, J.; Shin, C.; Kim, C.; Wojcik, A.; Hemmer, P. R.; Krueger, A.; Hanke, T.; Leitenstorfer, A.; Bratschitsch, R.; Jelezko, F.; Wrachtrup, J. *Nature* **2008**, *455*, 648−651.

(6) Grinolds, M. S.; Maletinsky, P.; Hong, S.; Lukin, M. D.; Walsworth, R. L.; Yacoby, A. *Nat. Phys.* **2011**, *7*, 687−692.

(7) Maletinsky, P.; Hong, S.; Grinolds, M. S.; Hausmann, B.; Lukin, M. D.; Walsworth, R. L.; Loncar, M.; Yacoby, A. *Nat. Nanotechnol.* **2012**, *7*, 320−4.

(8) Waldherr, G.; Wang, Y.; Zaiser, S.; Jamali, M.; SchulteHerbrüggen, T.; Abe, H.; Ohshima, T.; Isoya, J.; Du, J. F.; Neumann, P.; Wrachtrup, J. *Nature* **2014**, *506*, 204−207.

(9) Cramer, J.; Kalb, N.; Rol, M. A.; Hensen, B.; Blok, M. S.; Markham, M.; Twitchen, D. J.; Hanson, R.; Taminiau, T. H. *Nat. Commun.* **2016**, *7*, 1−7.

(10) Hensen, B.; et al. *Nature* **2015**, *526*, 682−686.

(11) Kalb, N.; Reiserer, A. A.; Humphreys, P. C.; Bakermans, J. J.; Kamerling, S. J.; Nickerson, N. H.; Benjamin, S. C.; Twitchen, D. J.; Markham, M.; Hanson, R. *Science* **2017**, *356*, 928−932.

(12) Humphreys, P. C.; Kalb, N.; Morits, J. P. J.; Schouten, R. N.; Vermeulen, R. F.; Twitchen, D. J.; Markham, M.; Hanson, R. *Nature* **2018**, *558*, 268−273.

(13) Abobeih, M. H.; Cramer, J.; Bakker, M. A.; Kalb, N.; Markham, M.; Twitchen, D. J.; Taminiau, T. H. *Nat. Commun.* **2018**, *9*, 1−8.

(14) Robledo, L.; Childress, L.; Bernien, H.; Hensen, B.; Alkemade, P. F. A.; Hanson, R. *Nature* **2011**, *477*, 574−578.

(15) Maurer, P. C.; Kucsko, G.; Latta, C.; Jiang, L.; Yao, N. Y.; Bennett, S. D.; Pastawski, F.; Hunger, D.; Chisholm, N.; Markham, M.; Twitchen, D. J.; Cirac, J. I.; Lukin, M. D. *Science* **2012**, *336*, 1283−1286.

(16) Taminiau, T. H.; Cramer, J.; Van Der Sar, T.; Dobrovitski, V. V.; Hanson, R. *Nat. Nanotechnol.* **2014**, *9*, 171−176.

(17) Englund, D.; Shields, B.; Rivoire, K.; Hatami, F.; Vučković, J.; Park, H.; Lukin, M. D. *Nano Lett.* **2010**, *10*, 3922−3926.

(18) Wolters, J.; Schell, A. W.; Kewes, G.; Nüsse, N.; Schoengen, M.; Döscher, H.; Hannappel, T.; Löchel, B.; Barth, M.; Benson, O. *Appl. Phys. Lett.* **2010**, *97*, 141108.

(19) Van Der Sar, T.; Hagemeier, J.; Pfaff, W.; Heeres, E. C.; Thon, S. M.; Kim, H.; Petroff, P. M.; Oosterkamp, T. H.; Bouwmeester, D.; Hanson, R. *Appl. Phys. Lett.* **2011**, *98*, 193103.

(20) Faraon, A.; Santori, C.; Huang, Z.; Acosta, V. M.; Beausoleil, R. G. *Phys. Rev. Lett.* **2012**, *109*, 2−6.

(21) Hausmann, B. J.; Shields, B. J.; Quan, Q.; Chu, Y.; De Leon, N. P.; Evans, R.; Burek, M. J.; Zibrov, A. S.; Markham, M.; Twitchen, D. J.; Park, H.; Lukin, M. D.; Loncar, M. *Nano Lett.* **2013**, *13*, 5791−5796.

(22) Lee, J. C.; Bracher, D. O.; Cui, S.; Ohno, K.; McLellan, C. A.; Zhang, X.; Andrich, P.; Alemán, B.; Russell, K. J.; Magyar, A. P.; Aharonovich, I.; Bleszynski Jayich, A.; Awschalom, D.; Hu, E. L. *Appl. Phys. Lett.* **2014**, *105*, 261101.

(23) Li, L.; Schröder, T.; Chen, E. H.; Walsh, M.; Bayn, I.; Goldstein, J.; Gaathon, O.; Trusheim, M. E.; Lu, M.; Mower, J.; Cotlet, M.; Markham, M. L.; Twitchen, D. J.; Englund, D. *Nat. Commun.* **2015**, *6*, 6173.

(24) Riedrich-Möller, J.; Pezzagna, S.; Meijer, J.; Pauly, C.; Mücklich, F.; Markham, M.; Edmonds, A. M.; Becher, C. *Appl. Phys. Lett.* **2015**, *106*, 221103.

(25) Faraon, A.; Barclay, P. E.; Santori, C.; Fu, K. M. C.; Beausoleil, R. G. *Nat. Photonics* **2011**, *5*, 301−305.

(26) Barclay, P. E.; Fu, K. M. C.; Santori, C.; Faraon, A.; Beausoleil, R. G. *Phys. Rev. X* **2011**, *1*, 1−7.

(27) Gould, M.; Schmidgall, E. R.; Dadgostar, S.; Hatami, F.; Fu, K. M. C. *Phys. Rev. Appl.* **2016**, *6*, 2−7.

(28) Kaupp, H.; Deutsch, C.; Chang, H. C.; Reichel, J.; Hänsch, T. W.; Hunger, D. *Phys. Rev. A: At., Mol., Opt. Phys.* **2013**, *88*, 1−8.

(29) Johnson, S.; Dolan, P. R.; Grange, T.; Trichet, A. A. P.; Hornecker, G.; Chen, Y. C.; Weng, L.; Hughes, G. M.; Watt, A. A. R.; Auffèves, A.; Smith, J. M. *New J. Phys.* **2015**, *17*, 122003.

(30) Riedel, D.; Söllner, I.; Shields, B. J.; Starosielec, S.; Appel, P.; Neu, E.; Maletinsky, P.; Warburton, R. J. *Phys. Rev. X* **2017**, *7*, 1−8.

(31) Rabl, P.; Kolkowitz, S. J.; Koppens, F. H.; Harris, J. G.; Zoller, P.; Lukin, M. D. *Nat. Phys.* **2010**, *6*, 602−608.

(32) Arcizet, O.; Jacques, V.; Siria, A.; Poncharal, P.; Vincent, P.; Seidelin, S. *Nat. Phys.* **2011**, *7*, 879−883.

DOI: 10.1021/acs.nanolett.9b01316
Nano Lett. 2019, 19, 3987−3992

(33) Kolkowitz, S.; Jayich, A. C. B.; Unterreithmeier, Q. P.; Bennett, S. D.; Rabl, P.; Harris, J. G. E.; Lukin, M. D. *Science* **2012**, *335*, 1603−1606.
(34) Kepesidis, K. V.; Bennett, S. D.; Portolan, S.; Lukin, M. D.; Rabl, P. *Phys. Rev. B: Condens. Matter Mater. Phys.* **2013**, *88*, 1−12.
(35) Golter, D. A.; Oo, T.; Amezcua, M.; Stewart, K. A.; Wang, H. *Phys. Rev. Lett.* **2016**, *116*, 1−6.
(36) Lee, D.; Lee, K. W.; Cady, J. V.; Ovartchaiyapong, P.; Jayich, A. C. B. *J. Opt.* **2017**, *19*, No. 033001.
(37) Ohno, K.; Joseph Heremans, F.; Bassett, L. C.; Myers, B. A.; Toyli, D. M.; Bleszynski Jayich, A. C.; Palmstrøm, C. J.; Awschalom, D. D. *Appl. Phys. Lett.* **2012**, *101*, No. 082413.
(38) Kim, E.; Acosta, V. M.; Bauch, E.; Budker, D.; Hemmer, P. R. *Appl. Phys. Lett.* **2012**, *101*, No. 082410.
(39) McLellan, C. A.; Myers, B. A.; Kraemer, S.; Ohno, K.; Awschalom, D. D.; Bleszynski Jayich, A. C. *Nano Lett.* **2016**, *16*, 2450−2454.
(40) Doherty, M. W.; Manson, N. B.; Delaney, P.; Hollenberg, L. C. L. *New J. Phys.* **2011**, *13*, 025019.
(41) Fu, K. M. C.; Santori, C.; Barclay, P. E.; Rogers, L. J.; Manson, N. B.; Beausoleil, R. G. *Phys. Rev. Lett.* **2009**, *103*, 1−4.
(42) Siyushev, P.; Pinto, H.; Vörös, M.; Gali, A.; Jelezko, F.; Wrachtrup, J. *Phys. Rev. Lett.* **2013**, *110*, 1−5.
(43) Bernien, H.; Childress, L.; Robledo, L.; Markham, M.; Twitchen, D.; Hanson, R. *Phys. Rev. Lett.* **2012**, *108*, No. 043604.
(44) Bernien, H.; Hensen, B.; Pfaff, W.; Koolstra, G.; Blok, M. S.; Robledo, L.; Taminiau, T. H.; Markham, M.; Twitchen, D. J.; Childress, L.; Hanson, R. *Nature* **2013**, *497*, 86−90.
(45) See Supporting Information for additional data, as well as details on sample fabrication, measurement sequences and data analysis.
(46) Pezzagna, S.; Rogalla, D.; Wildanger, D.; Meijer, J.; Zaitsev, A. *New J. Phys.* **2011**, *13*, No. 035024.
(47) Janitz, E.; Ruf, M.; Dimock, M.; Bourassa, A.; Sankey, J.; Childress, L. *Phys. Rev. A: At., Mol., Opt. Phys.* **2015**, *92*, 1−11.
(48) Bogdanović, S.; van Dam, S. B.; Bonato, C.; Coenen, L. C.; Zwerver, A.-M. J.; Hensen, B.; Liddy, M. S. Z.; Fink, T.; Reiserer, A.; Lončar, M.; Hanson, R. *Appl. Phys. Lett.* **2017**, *110*, 171103.
(49) van Dam, S. B.; Ruf, M.; Hanson, R. *New J. Phys.* **2018**, *20*, 115004.
(50) van Dam, S. B.; Walsh, M.; Degen, M. J.; Bersin, E.; Mouradian, S. L.; Galiullin, A.; Ruf, M.; IJspeert, M.; Taminiau, T. H.; Hanson, R.; Englund, D. R. *Phys. Rev. B: Condens. Matter Mater. Phys.* **2019**, *99*, 161203.
(51) Campbell, B.; Mainwood, A. *physica status solidi (a)* **2000**, *181*, 99−107.
(52) Orwa, J. O.; Santori, C.; Fu, K. M. C.; Gibson, B.; Simpson, D.; Aharonovich, I.; Stacey, A.; Cimmino, A.; Balog, P.; Markham, M.; Twitchen, D.; Greentree, A. D.; Beausoleil, R. G.; Prawer, S. *J. Appl. Phys.* **2011**, *109*, No. 083530.
(53) Chu, Y.; et al. *Nano Lett.* **2014**, *14*, 1982−1986.
(54) Hausmann, B. J. M.; Khan, M.; Zhang, Y.; Babinec, T. M.; Martinick, K.; McCutcheon, M.; Hemmer, P. R.; Loncar, M. *Diamond Relat. Mater.* **2010**, *19*, 621−629.
(55) Petráková, V.; Taylor, A.; Kratochvílová, I.; Fendrych, F.; Vacík, J.; Kučka, J.; Šturs̆a, J.; Cígler, P.; Ledvina, M.; Fišerová, A.; Kneppo, P.; Nesládek, M. *Adv. Funct. Mater.* **2012**, *22*, 812−819.
(56) Grillo, S. E.; Field, J. E. *J. Phys. D: Appl. Phys.* **1997**, *30*, 202−209.
(57) Atikian, H. A.; Eftekharian, A.; Jafari Salim, A.; Burek, M. J.; Choy, J. T.; Hamed Majedi, A.; Lončar, M. *Appl. Phys. Lett.* **2014**, *104*, 122602.
(58) Lee, C. L.; Gu, E.; Dawson, M. D.; Friel, I.; Scarsbrook, G. A. *Diamond Relat. Mater.* **2008**, *17*, 1292−1296.
(59) Challier, M.; Sonusen, S.; Barfuss, A.; Rohner, D.; Riedel, D.; Koelbl, J.; Ganzhorn, M.; Appel, P.; Maletinsky, P.; Neu, E. *Micromachines* **2018**, *9*, 148.
(60) Tao, Y.; Boss, J. M.; Moores, B. A.; Degen, C. L. *Nat. Commun.* **2014**, *5*, 1−8.
(61) Riedel, D.; Rohner, D.; Ganzhorn, M.; Kaldewey, T.; Appel, P.; Neu, E.; Warburton, R. J.; Maletinsky, P. *Phys. Rev. Appl.* **2014**, *2*, 1−6.
(62) Appel, P.; Neu, E.; Ganzhorn, M.; Barfuss, A.; Batzer, M.; Gratz, M.; Tschöpe, A.; Maletinsky, P. *Rev. Sci. Instrum.* **2016**, *87*, No. 063703.
(63) Bogdanović, S.; Liddy, M. S. Z.; van Dam, S. B.; Coenen, L. C.; Fink, T.; Lončar, M.; Hanson, R. *APL Photonics* **2017**, *2*, 126101.
(64) Volpe, P.; Muret, P.; Omnes, F.; Achard, J.; Silva, F.; Brinza, O.; Gicquel, A. *Diamond Relat. Mater.* **2009**, *18*, 1205−1210.
(65) Friel, I.; Clewes, S. L.; Dhillon, H. K.; Perkins, N.; Twitchen, D. J.; Scarsbrook, G. A. *Diamond Relat. Mater.* **2009**, *18*, 808−815.
(66) Naamoun, M.; Tallaire, A.; Silva, F.; Achard, J.; Doppelt, P.; Gicquel, A. *Phys. Status Solidi A* **2012**, *209*, 1715−1720.
(67) Briegel, H.-J.; Dür, W.; Cirac, J. I.; Zoller, P. *Phys. Rev. Lett.* **1998**, *81*, 5932−5935.
(68) Rozpędek, F.; Goodenough, K.; Ribeiro, J.; Kalb, N.; Vivoli, V. C.; Reiserer, A.; Hanson, R.; Wehner, S.; Elkouss, D. *Quantum Science and Technology* **2018**, *3*, No. 034002.
(69) Rozpędek, F.; Yehia, R.; Goodenough, K.; Ruf, M.; Humphreys, P. C.; Hanson, R.; Wehner, S.; Elkouss, D. *Phys. Rev. A: At., Mol., Opt. Phys.* **2019**, *99*, 1−29.

DOI: 10.1021/acs.nanolett.9b01316
Nano Lett. 2019, 19, 3987−3992